Materials Science and Engineering A 528 (2011) 6121–6127

Contents lists available at ScienceDirect

Materials Science and Engineering A

journal homepage: www.elsevier.com/locate/msea

Variations in overall- and phase-hardness of a new Ni-based superalloy during isothermal aging

Jun-Hak Oh, In-Chul Choi, Yong-Jae Kim, Byung-Gil Yoo, Jae-il Jang*

Division of Materials Science and Engineering, Hanyang University, Seoul 133-791, Republic of Korea

ARTICLE INFO

Article history:
Received 6 January 2011
Received in revised form 6 March 2011
Accepted 31 March 2011
Available online 23 April 2011

Keywords:
Ni-based superalloy
Inconel 740
Nanoindentation
Precipitation strengthening
Aging

ABSTRACT

Influence of isothermal aging on the microstructures and hardness in Inconel 740, a relatively new Ni-based superalloy, was explored using the specimens aged at 810 °C for different times. As aging time increased, the size of gamma prime precipitates continuously increased while their fraction remained almost constant. Nanoindentation experiments revealed that the overall hardness increased till the aging time of 100 h and then decreased with the aging time. Estimation of phase hardness by applying a simple rule-of-mixture showed that, with aging time, the hardness of gamma matrix decreased whereas that of gamma prime precipitates increased. The aging-induced strength change is discussed in terms of the possible contributions of precipitation strengthening and solid solution strengthening.

1. Introduction

The Inconel 740, a relatively new member of Ni-based superalloy family, was developed for the applications to steam boiler tubing in 'Advanced Ultra-SuperCritical (A-USC)' fossil power plants [1–4]. Since the target steam condition of the new boiler system is above 375 bar and 700 °C, this alloy was designed to have excellent performances (such as good microstructure stability, high resistance to coal-ash-corrosion/oxidation, and high creep-rupture strength) at high temperature up to 770 °C [1–4].

Like many other Ni-based superalloys, Inconel 740 is primarily strengthened by the precipitation of very fine gamma prime (γ′) (having an ordered face-centered cubic structure) in the disordered gamma (γ) matrix [1–4]. It is generally accepted that the precipitation strengthening in Ni-based superalloys is mainly controlled by cutting mechanism rather than bowing (or typically referred to as Orowan) mechanism [5]: while a pair of $a/2\langle 1\ \bar{1}\ 0\rangle\{1\,1\,1\}$ dislocations passes through the γ/γ′ structure, the first dislocation enters the spherical γ′ precipitates with the formation of an anti-phase boundary (APB) and the following dislocation removes it [6]. This type of cutting mechanism can be roughly subdivided into two groups; weakly coupled dislocations (WCD or weak pair-coupling) model [7] and strongly coupled dislocations (SCD or strong pair-coupling) model [8]. In superalloys, the former is typically applied to the case that the size and volume fraction of γ′ are small [7], whereas the latter is known to be more appropriate for the case that the spacing of the dislocation pairs becomes comparable to the particle diameter [8].

Ni-based superalloys inevitably experience various microstructural changes during their high temperature service life, such as γ′ coarsening, formation of topologically close-packed (TCP) phase, and increasing carbides contents (mostly $M_{23}C_6$) [9–12]. Thus, the influence of aging on the microstructure and mechanical properties of Ni-based superalloys have been studied extensively over the past decades [1,3,4,9–12]. However, limited efforts have been made on the topic for Inconel 740. In addition, to our best knowledge, there has been no attempt to analyze the role of each phase in the strength change in detail. With this in mind, in this study, we have explored how the overall hardness as well as phase hardness of Inconel 740 can be affected by the isothermal aging. Results are discussed in terms of aging-induced changes in the contributions of precipitation strengthening and solid solution strengthening in this new superalloy.

2. Experiments

Examined material is a commercial grade Inconel 740 (produced at Special Metals Corporation) whose nominal chemical composition (in wt.%) is 0.03C–25Cr–0.5Mo–20Co–0.9Al–1.8Ti–2Nb–0.3Mn–0.7Fe–0.5Si with the balance Ni. Since the dissolution temperature of γ′ precipitates in this alloy is known to be 821 °C [1], samples were isothermally aged at 810 °C for different times (100, 200, 500 and 1000 h) and compared with as-received sample. The average grain

* Corresponding author. Tel.: +82 2 2220 0402; fax: +82 2 2220 0389.
E-mail address: jijang@hanyang.ac.kr (J.-i. Jang).

0921-5093/$ – see front matter © 2011 Elsevier B.V. All rights reserved.
doi:10.1016/j.msea.2011.03.115

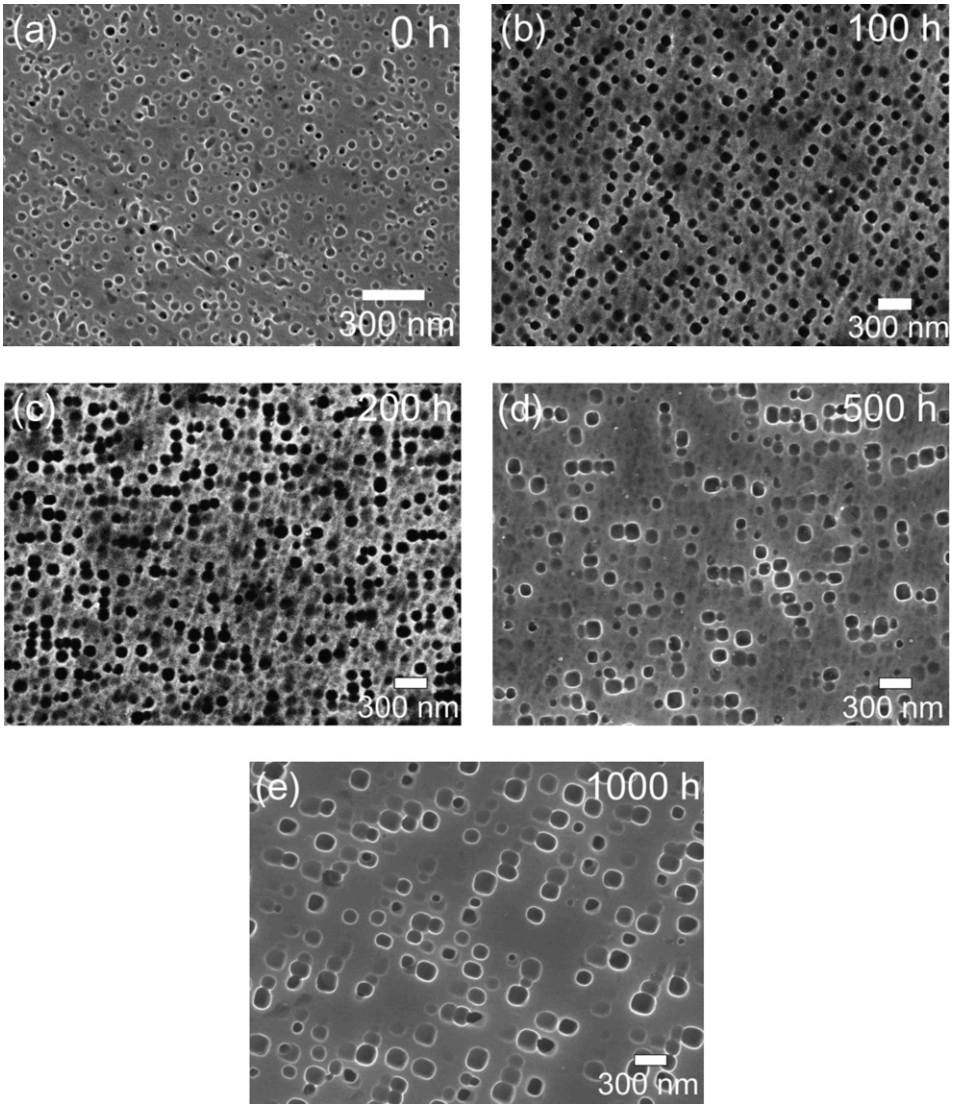

Fig. 1. SEM micrographs used for measuring the fraction of γ′ precipitate (chemically etched samples) in the samples aged for (a) 0 h; (b) 100 h; (c) 200 h; (d) 500 h; (e) 1000 h.

size in the as-received sample was about 150 μm which is larger than nominal grain size in the literature [1].

Microstructural change due to aging was examined by using field emission scanning electron microscopy, FE-SEM (JSM-6340F, JEOL Ltd., Tokyo, Japan). With the SEM micrographs, the size and fraction of γ′ were quantitatively measured using an image analyzer software (Image-pro, Media Cybernetics Inc., Bethesda, MD). An electrical etching (at 10 V for 90 s in a solution of 10 ml perchloric acid, 30 ml propionic acid and 40 ml ethanol) and a chemical etching (for 10 s in a solution of 33 ml nitric acid and 66 ml hydrochloric acid) were adopted for measuring the size and fraction of γ′ respectively. Adoption of different methods was because the electrical etching (that selectively etches out the γ matrix having a large fraction) could induce an overestimation of γ′ fraction, whereas the chemical etching (that selectively etches out the γ matrix) could result in an overestimation of γ′ size.

The transmission electron microscopy (TEM) characterization was performed on selected samples with a CM-30 (Philips Electronic Corp., Mahwah, NJ) operating at 200 keV. Energy dispersive X-ray microanalysis was performed using a Link Pentafet energy-dispersive spectrometer (EDS) with an ultra thin window, controlled using the Link eXL system. To prepare TEM thin foils, thin sheet were cut out using a low-speed diamond saw and were mechanically thinned down to about 100 μm in thickness using a SiC paper of #1000. Discs having a diameter of 3 mm were punched out of the thin sheets and electropolished to perforation with an 800 ml methanol and 200 ml perchloric acid electrolyte at −50 °C and 20 V, using a double-jet electro polisher.

To investigate the aging-induced hardness change, nanoindentation experiments were carried out using a Nanoindenter-XP (MTS System Corp., Oak Ridge, TN) with a common Berkovich indenter. During the test, the sample was loaded up to the peak load (P_{max}) of 3 mN under a constant strain rate of 0.05 s^{-1}. The tip calibration and the hardness calculation were conducted in accordance with the Oliver–Pharr method [13]. The specimen surfaces were initially ground with fine SiC paper of #2000 and to avoid artifacts related to a hardened surface layer, indentation tests were made on electro-polished surface instead of mechanically polished one. Electrical polishing was conducted in a solution of 850 ml methanol and 150 ml hydrochloric acid at a room temperature and 40 V for 20 s.

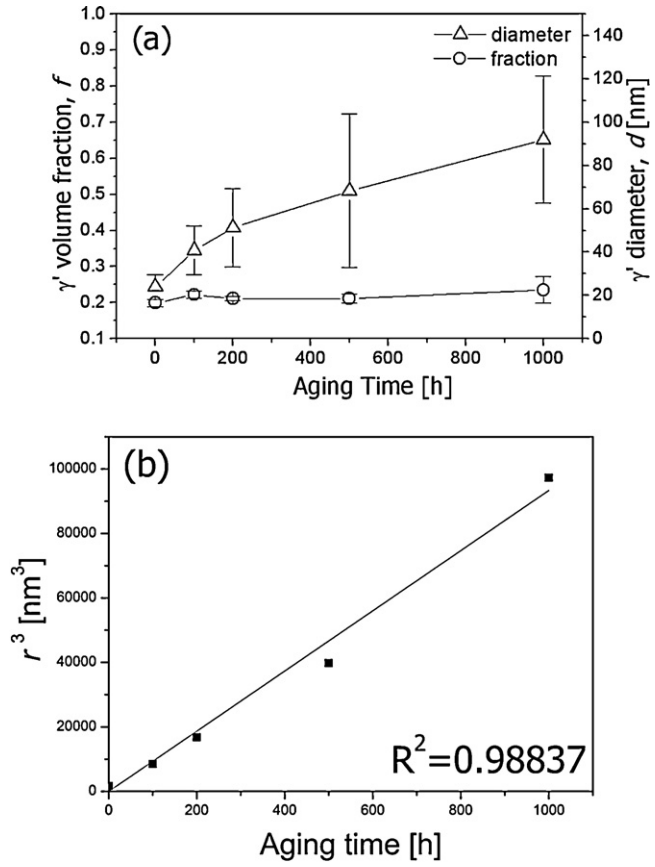

Fig. 2. Microstructural change of γ′ precipitates; (a) variation in fraction and diameter; (b) LSW analysis of γ′ coarsening.

3. Results and discussion

3.1. Microstructural change

Representative SEM micrographs for the aged samples are shown in Fig. 1 where all samples exhibited uniform dispersion of γ′ precipitates in γ matrix. Two types of changes in the precipitates are notable in the figure. First, the size of the γ′ precipitates increased with aging time, which will be discussed below. Second, as the aging time increased, the morphology of γ′ precipitates changed from a spherical shape to a rounded cubic form. The formation of rounded cubic γ′ may be attributed by the medium degree of γ–γ′ lattice mismatch. Nevertheless, if compared to other Ni-based superalloys, the shape change is not significant and this relatively higher stability of γ′ precipitates in Inconel 740 is known to be beneficial to the mechanical performance (such as rupture strength at 750 °C) during high-temperature service [1].

Using the high-resolution SEM images, the size and fraction of γ′ were quantitatively investigated. For each aging condition, at least 6 micrographs were used for measuring the γ′ fraction, and more than 150 precipitates were examined for estimating the diameter of the γ′ precipitates. The results are summarized in Fig. 2(a) where it is shown that, with increasing aging time, the size of γ′ continuously increased whereas their fraction was not seriously changed. The aging-induced coarsening of γ′ precipitates could be described by Lifshitz–Slyozov–Wagner (LSW) theory for which coarsening process is driven by reduction in total interfacial energy and thus growth kinetics would follow an equation given as

$$r^3 - r_0{}^3 = kt \tag{1}$$

where r is the averaged radius of the precipitates at time t, r_0 is the initial size, and k is the rate constant. In Fig. 2(b), it is seen that the plot of r^3 vs. time in the present study is following the relation in Eq. (1).

To analyze other-typed precipitates, microstructures nearby grain boundaries (which are good places for heterogeneous nucleation of other precipitates) in each sample were examined, as shown in Fig. 3. While almost no precipitate was found in the as-received sample [Fig. 3(a)], the $M_{23}C_6$ carbide precipitates were obviously observed at grain boundaries after aging for 100 h [Fig. 3(b)]. In 200-h-aged sample, small quantity of a needle-like eta (η) phase was found mainly nearby grain boundaries [Fig. 3(c)]. The η phase and $M_{23}C_6$ carbide continuously grew during aging [Fig. 3(d)].

The $M_{23}C_6$ carbides are known to be formed by the decomposition of MC carbide decomposition reaction that is frequently written in the literature as

$$MC + \gamma \rightarrow M_{23}C_6 + \gamma'.$$

This is based on the observations that both $M_{23}C_6$ and γ′ typically form in the area surrounding the degenerated MC carbide [9,11,12,14]. Examination of TEM diffraction patters and EDS spectra suggested that MC and $M_{23}C_6$ carbides (which are major carbides of Inconel 740) [3] are (Nb,Ti)C- and $Cr_{23}C_6$-type carbide, respectively [see Fig. 4(a) and (b)]. As the MC carbide decomposition reaction proceeds, the MC acts as the source of C and Ti in $M_{23}C_6$ carbides while the γ matrix serves as the source of their Ni, Al and Cr [12]. In addition, as shown in Fig. 4(c), η phase was found to be hexagonal close-packed Ni_3(Ti,Nb). Lvov et al. [9] reported that the growth of η phase might occur at the expense of the γ′ precipitate because there was a γ′ precipitate denuded region surrounding η phase.

3.2. Overall hardness change

Nanoindentation experiments were conducted to investigate the aging-induced variation in the hardness H (which is called 'overall hardness' below, to differentiate it from 'phase' hardness). The results are provided in Fig. 5 in which the overall hardness was found to rapidly increase between as-received and 100-h-aged samples, and then continuously decreased with aging time.

In order to analyze how much the precipitation of γ′ affects the overall hardness variation, the contributions of both cutting and Orowan (bowing) mechanism responsible for precipitation strengthening were estimated in terms of the critical resolved shear stress (CRSS). Precipitation strengthening in a superalloy is usually controlled by cutting mechanism that can be subdivided into two models, i.e., weakly coupled dislocations (WCD) model for small precipitates [7] and strongly coupled dislocations (SCD) model for large precipitates [8]. For both cases, it is possible to estimate the CRSS necessary for cutting the precipitates based on the assumptions that a pair of edge dislocations travels in the ⟨1 1 0⟩ direction on the {1 1 1} plane and cut through the ordered γ′ precipitates in a disordered matrix.

In the case of WCD model appropriate for small precipitates, the CRSS can be given as [7]

$$\tau_{\mathrm{ppt,WCD}} = \frac{1}{2}\left(\frac{\gamma_{\mathrm{APB}}}{b}\right)^{3/2}\left(\frac{bdf}{T}\right)^{1/2} A - \frac{1}{2}\left(\frac{\gamma}{b}\right) f \tag{2}$$

where γ_{APB} is anti-phase boundary energy (APBE) of the γ′ in the {1 1 1} plane, b is the Burgers vector of edge dislocation in the matrix, d the precipitate diameter, f the volume fraction of the γ′ precipitates, T the line tension of the dislocation, and A a numerical factor depending on the morphology of the precipitates (that is 0.72 for spherical precipitates) [5].

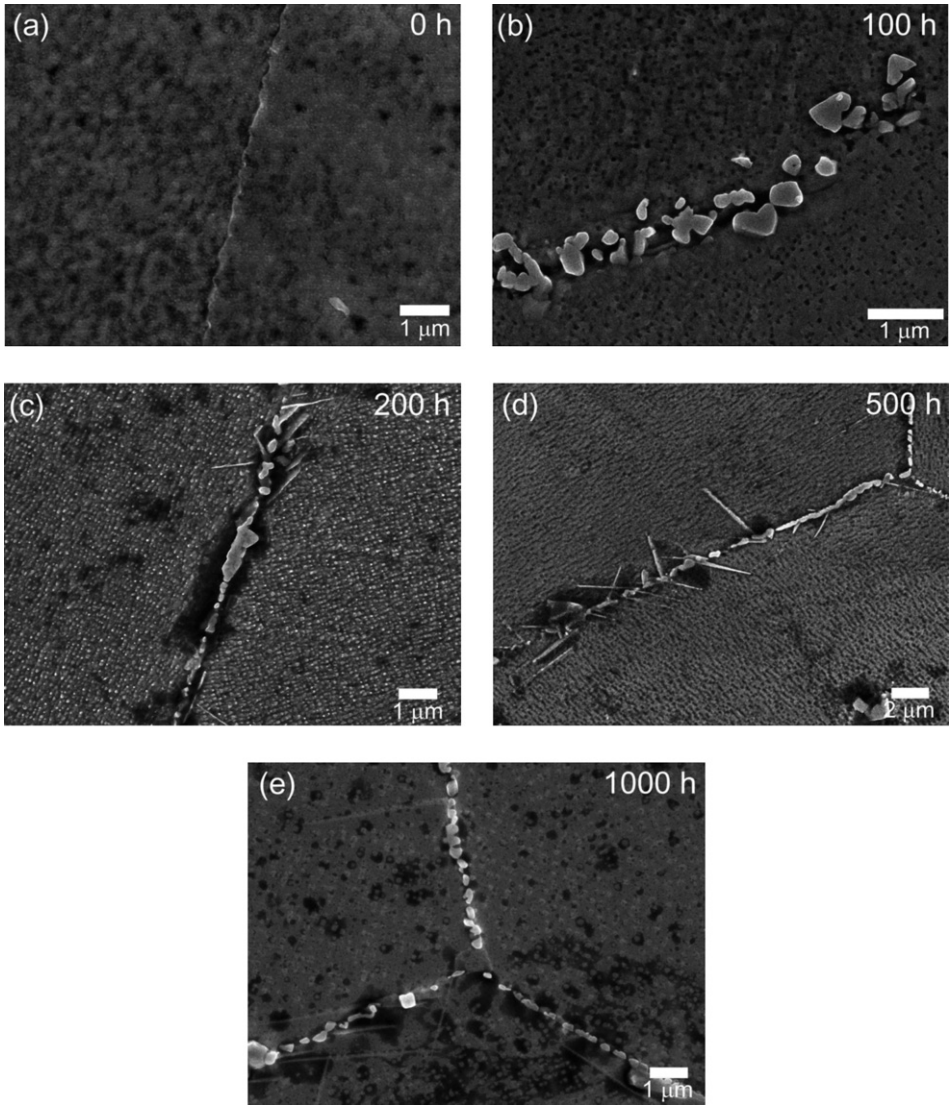

Fig. 3. Precipitation behavior near grain boundaries of the samples aged for (a) 0 h; (b) 100 h; (c) 200 h; (d) 500 h; (e) 1000 h.

For SCD model applicable to larger precipitates, the CRSS can be obtained by [8]

$$\tau_{\mathrm{ppt,SCD}} = \left(\frac{\sqrt{3}}{2}\right)\frac{Tf^{1/2}w}{bd}\left(1.28\frac{d\gamma_{\mathrm{APB}}}{wT} - 1\right)^{1/2} \quad (3)$$

where w is a constant (of the order of unity) which accounts for the elastic repulsion between the strongly paired dislocations [5] and is considered as unity in this work. In order to calculate Eqs. (2) and (3), the value of b, γ_{APB}, G, and T should be known; In present study, b and γ_{APB} were taken as 0.254 nm and 0.28 J m^{-2}, respectively [15]. The shear modulus G [$=0.5E/(1+\nu)$] was calculated using elastic modulus $E = 221$ GPa (of Inconel 740) and Poisson's ratio $\nu = 0.35$ [16], and T was estimated as $0.5Gb^2$ [7].

Although the cutting mechanism is known to be pre-dominant mechanism for the precipitation strengthening in a superalloy, previous works [14] reported that, in a limited condition (e.g., for large precipitates in an overaged condition), precipitation strengthening of superalloys can be also controlled by Orowan mechanism. It is well accepted that the CRSS necessary for Orowan mechanism can be expressed as [17]

$$\tau_{\mathrm{ppt,Oro}} = \frac{Gb}{\lambda} \quad (4)$$

where λ is interparticle spacing between precipitates and is often simplified as

$$\lambda = \frac{2(1-f)d}{3f} \quad (5)$$

where f is the volume fraction of precipitates and d is the diameter of the spherical precipitate. Since these f was already obtained experimentally (see Fig. 2(a)), the CRSS for Orowan mechanism can be easily evaluated according to Eqs. (4) and (5).

With the values of the CRSS calculated according to Eqs. (2)–(4), one can estimate the contribution of each strengthening mechanism to the measured overall hardness. The calculated CRSS for each strengthening mechanism (τ_{ppt}) was plotted against the precipitate diameter, which is given in Fig. 6(a). For this theoretical calculation, the fraction of precipitates was fixed as average values for each sample [see Fig. 2(a)]. In the figure, for a given diameter, the mechanism showing the lowest CRSS is supposed to mainly contribute to the strengthening. With increasing precipitate size, there is a transition of the governing mechanism from WCD cutting to Orowan mechanism. The SCD cutting mechanism could be ruled out for entire range of precipitate diameter. The maximum CRSS (at the transition point from the WCD cutting curve to Orowan curve) indicates the maximum possible amount of the

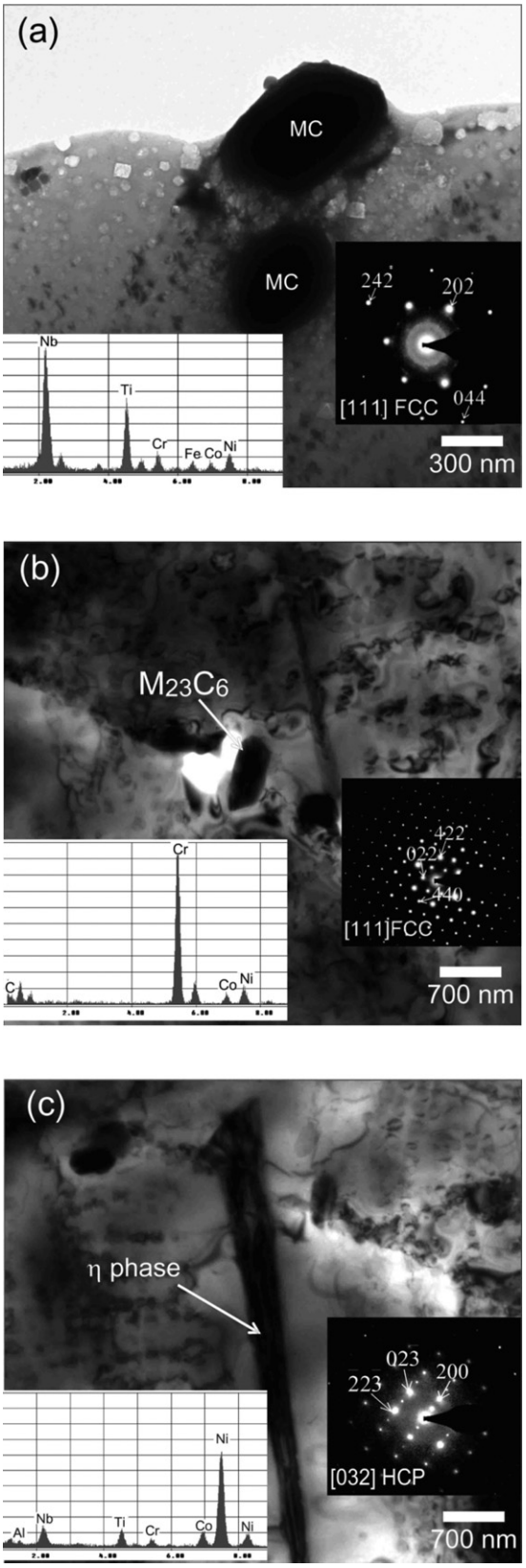

Fig. 4. TEM images and EDS spectra of other precipitates; (a) MC carbide; (b) $M_{23}C_6$ carbide; (c) η phase.

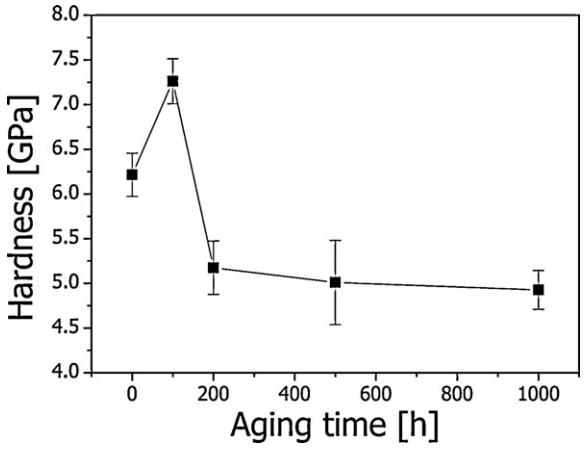

Fig. 5. Variation in the overall hardness with aging time.

precipitate strengthening. Therefore, it is expected from Fig. 2(a) that, as the average diameter (d) of precipitates increases, the strength of the superalloy increases till critical diameter d_{crit} (that is about 35–40 nm in the present work) and then decreases. This may explain the highest overall hardness of the 100-h-aged sample in Fig. 5, since the sample exhibits the average diameter of around 40 nm [see Fig. 2(a)].

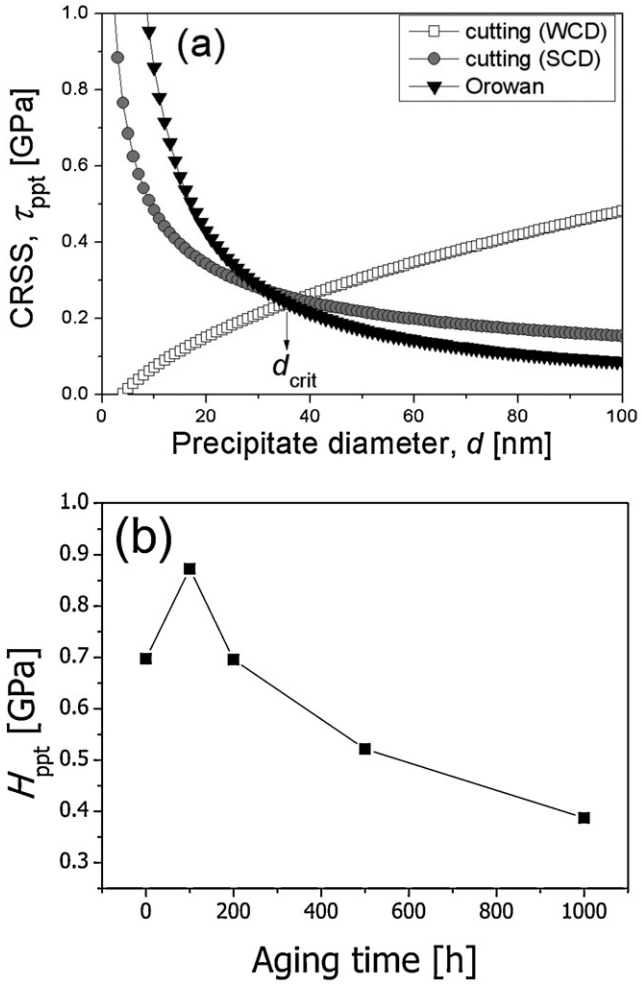

Fig. 6. Analysis of precipitation strengthening; (a) analytical calculations of CRSS vs. precipitate diameter; (b) contributing amount of precipitation strengthening to overall hardness.

By applying Tabor's relationship and von Mises flow rule, the CRSS values for each strengthening mechanism (τ_{ppt}) can be converted into the amount of hardness increase due to the precipitation strengthening, H_{ppt} [18]:

$$H_{ppt} = 3\sigma_{ppt} = 3\sqrt{3}\tau_{ppt}. \quad (6)$$

The variation in the calculated H_{ppt} is provided in Fig. 6(b). Similar trend of the H_{ppt} in Fig. 6(a) to that of the overall hardness H in Fig. 5 may imply that the change in the contribution of γ' precipitation strengthening plays conceivably the most important role in the variation in overall strength with aging.

3.3. Phase hardness change

Now, we turn our attention into the phase hardness of γ and γ' for better understanding the strength change during aging. Although some previous works have directly measured the phase hardness in Ni-based superalloys through nanoindentation experiments [19], here the size of γ' precipitates in as-received sample is very small (about 30 nm) and thus it is almost impossible to directly measure their phase hardness. To overcome this difficulty, we adopted a simple rule-of-mixture to obtain the phase hardness as follows. Although the rule-of-mixture may not hold valid in some cases, it is popularly used for analyzing the connection between the strength (or hardness) of constituent phase and the macroscopic overall strength in crystalline or amorphous alloys (for recent example, see [20–22]).

As the first step, the basic hardness H_0 is defined as the hardness without contribution of precipitation strengthening and thus can be given as

$$H_0 = H - H_{ppt}. \quad (7)$$

Here H is the measured overall hardness and H_{ppt} is the amount of hardness increase due tothe precipitation, as discussed above. Thus, H_0 could be estimated by putting H in Fig. 5 and H_{ppt} in Fig. 6(b) into Eq. (7). Then, a simple rule-of-mixture was adopted to establishment of the relation between H_0 and hardness of each phase;

$$H_0 = V_\gamma H_\gamma + V_{\gamma'} H_{\gamma'} = (1 - V_{\gamma'})H_\gamma + V_{\gamma'} H_{\gamma'} \quad (8)$$

where V_γ and $V_{\gamma'}$ denote the volume fraction of γ and γ', respectively. The volume fraction of γ' precipitates $V_{\gamma'}$ was determined using SEM images: first, a big mark was introduced in the interesting area and a SEM image of the region near the mark was taken before indentations were made [Fig. 7(a)]. Note that the overall hardness H values in Fig. 5 were obtained from these indentations. Near the mark, nanoindentation tests were carried out and then SEM images of the hardness impressions were obtained [Fig. 7(b)]. Now, it is necessary to consider the size of the indentation-induced plastic zone, which should be much larger than the triangular impression area. According to Johnson's expanding-cavity model for elastic–plastic indentation with a cone [23], the plastic zone radius (r_p) can be estimated as:

$$r_p = a\left\{\frac{1}{6(1-\nu)}\left[\frac{E}{\sigma_y}\tan\beta + 4(1-2\nu)\right]\right\}^{1/3} \quad (9)$$

where a is the contact radius, β is the angle of inclination of the conical indenter to the surface, E is Young's modulus, ν is Poisson's ratio, and σ_y is the yield strength. In order to relate this conical indentation model to the present results, we adopted a general assumption that similar behavior is obtained when the angle of the cone gives the same area-to-depth relation as the pyramid. For the Berkovich indenter (whose centerline-to-face angle is 65.3°), the equivalent cone angle is 70.3° and thus β is 19.7°. By putting the values, E = 221 GPa, σ_y = 721 MPa, ν = 0.35, and the contact radius (determined by the Oliver–Pharr method [13]) into the right hand term of Eq. (9), we could estimate the plastic zone radius. With the results, the $V_{\gamma'}$ was easily obtained by drawing a circle of plastic zone on the SEM images and analyzing the phase fraction using image analysis software, as shown in Fig. 7(c).

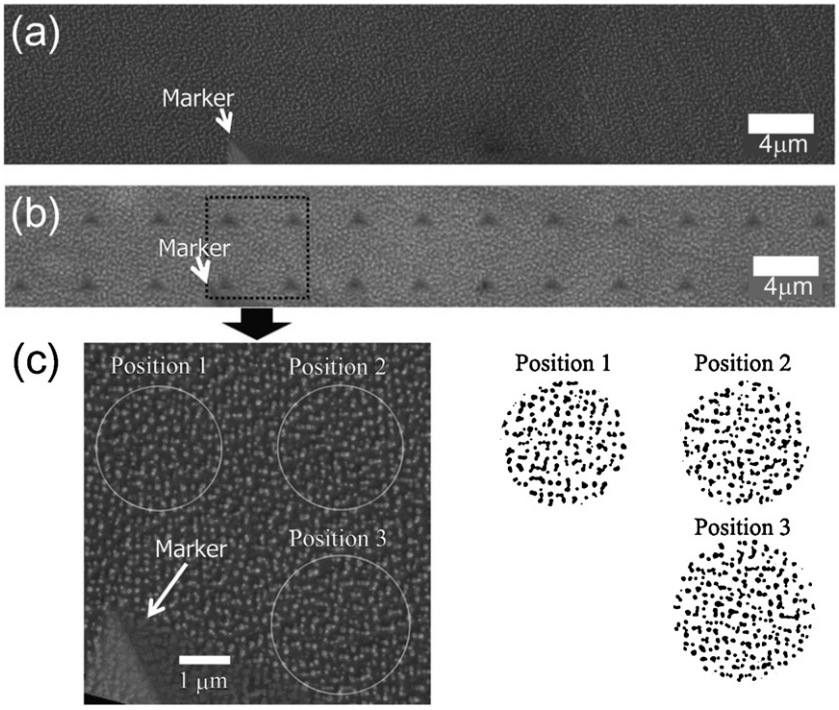

Fig. 7. Representative examples of the images used for applying a rule-of-mixture to the estimation of phase hardness from overall hardness; (a) before and (b) after indentation test; (c) calculation of volume fraction.

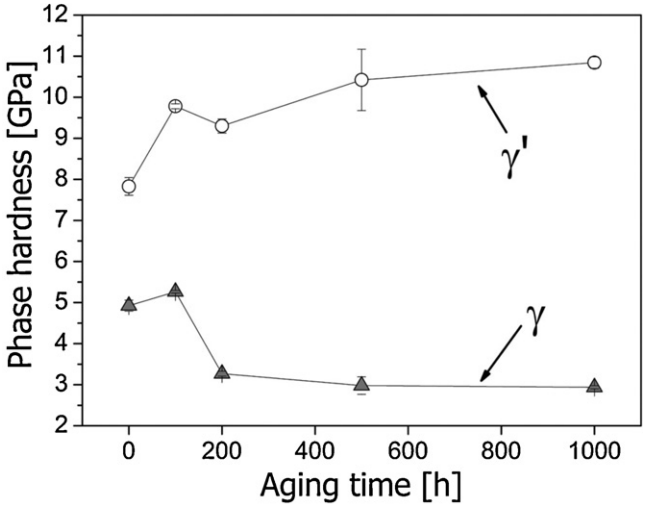

Fig. 8. Variation in phase hardness of matrix and γ′ precipitate.

Table 1
Measured compositions of γ and γ′ phases in the as-received, 100-h-aged, and 1000-h-aged samples.

Phases	Ni	Cr	Co	Nb	Al	Ti	Fe	Si
γ								
AR	40.1	32.9	19.2	1.7	2.2	0.8	1.4	1.7
100 h	39.5	33.9	19.9	1.7	1.4	1.2	0.8	1.7
1000 h	38.3	30.7	21.3	1.1	1.2	0.8	–	–
γ′								
AR	51.2	17.6	12.6	4.3	5.9	6.1	0.9	1.4
100 h	55.8	14.1	11.7	4.1	6.8	6.7	0.8	–
1000 h	56.4	5.1	8.0	10.0	11.3	9.1	–	–

With the H_0 (estimated by Eq. (7)) and the measured $V_{\gamma'}$, the hardness of each phase (i.e., H_γ and $H_{\gamma'}$) was obtained by applying Eq. (8) with the least-square analysis method. The results are summarized in Fig. 8. For all the cases, the hardness of γ′ precipitate (8–11 GPa) is much higher than that of γ matrix (2–5 GPa). This difference in hardness between the two phases is in agreement with the results by Göken et al. [19] who directly measured the hardness of each phase in Ni-based superalloys CMSX-6 and Waspaloy. Note again that, in the present work, such a direct measurement is almost impossible due to the very small size of the precipitates in Inconel 740.

It is interesting that the hardness change of γ′ precipitate and γ matrix exhibit opposite trends, i.e., with aging time, it appears that the $H_{\gamma'}$ continuously increases whereas H_γ is gradually decreasing. To find out the reason for the phase hardness variation, the chemical composition of as-received, 100-h and 1000-h-aged sample was investigated using EDS in TEM, as listed in Table 1. In γ matrix, the amounts of Cr, Nb and Al (which are known as solid-solution strengtheners) were reduced with aging time, which may cause the decrease in the H_γ. The change in the matrix composition might be related with (1) the formation of other phases like $M_{23}C_6$ carbides and η phases both of which are formed during aging, and (2) the relative change in the composition of γ′ precipitates. The discrete $M_{23}C_6$ particles formed at grain boundaries may withdraw solid solution strengthening elements (such as Cr) from the matrix [11], while the nucleation and growth of η phase (Ni_3(Ti,Nb)) progress with consuming the Nb in the matrix. In γ′ precipitates, the amount of Nb, Al and Ti increased with aging time, which may be responsible for the hardness increase.

From above analysis, one may completely understand the mechanism for the overall hardness change in Fig. 5. The increase in hardness between as-received and 100-h-aged sample might be mainly due to the increase in the contribution of precipitation strengthening [Fig. 6(b)]. The large decrease in the overall hardness after 100 h is conceivably caused by the decrease in the contributions of both precipitation strengthening by γ′ [Fig. 6(b)] and solid solution strengthening in γ matrix (Fig. 8).

4. Conclusion

Influence of isothermal aging on the microstructures and hardness in Inconel 740 was explored using the specimens aged at 810 °C for different times. Microstructural analysis revealed that, with increasing aging time, the size of γ′ precipitates continuously increased following the LSW theory but their fraction was not significantly changed. Nanoindentation experiments exhibited that the overall hardness increased until the aging time of 100 h, however, after then, largely decreased with aging time. Estimation of phase hardness by applying a simple rule-of-mixture showed that, with aging time, the hardness of γ matrix decreased and that of γ′ precipitates increased. From EDS analysis, it was found that the mechanical degradation in the matrix may be due to the reduction of solid solution strengthener amount of the γ matrix. Based on above results, the overall hardness change with aging was discussed in terms of the possible precipitation strengthening and solid solution strengthening.

Acknowledgments

This work was supported by the Human Resources Development of the Korea Institute of Energy Technology Evaluation and Planning (KETEP) grant funded by the Korea government Ministry of Knowledge Economy (No. 20101020300460). We thank Dr. M.L. Santella at ORNL for providing the valuable sample.

References

[1] S. Zhao, X. Xie, G.D. Smith, S.J. Patel, Mater. Sci. Eng. A 355 (2003) 96–105.
[2] N.D. Evans, P.J. Maziasz, R.W. Swindeman, G.D. Smith, Scripta Mater. 51 (2004) 503–507.
[3] S. Zhao, X. Xie, G.D. Smith, S.J. Patel, Mater. Des. 27 (2006) 1120–1127.
[4] C.J. Cowen, J. Mater. Eng. Perform., doi:10.1007/s11665-010-9731-0.
[5] B. Reppich, Acta Metall. 30 (1982) 87–94.
[6] E. Nembach, Particle Strengthening of Metals and Alloys, John Wiley and Sons, New York, 1997.
[7] L.M. Brown, R.K. Ham, Strengthening Mechanism in Crystals, Applied Science, London, 1971.
[8] W. Huther, B. Reppich, Z. Metall. 69 (1978) 628–634.
[9] G. Lvov, V.I. Levit, M.J. Kaufman, Metall. Mater. Trans. A 35A (2004) 1669–1679.
[10] C.-S. Han, J.-W. Kim, Y.-W. Kim, J. Korean Inst. Met. Mater. 47 (2009) 147–154.
[11] X.Z. Qin, J.T. Guo, C. Yuan, J.S. Hou, H.Q. Ye, Mater. Lett. 62 (2008) 2275–2278.
[12] X.Z. Qin, J.T. Guo, C. Yuan, C.L. Chen, H.Q. Ye, Metall. Mater. Trans. A 38A (2007) 3014–3022.
[13] W.C. Oliver, G.M. Pharr, J. Mater. Res. 7 (1992) 1564–1583.
[14] C.T. Sims, N.S. Stoloff, W.C. Hagel, Superalloys II, John Wiley and Sons, New York, 1987.
[15] M.P. Jackson, R.C. Reed, Mater. Sci. Eng. A 259 (1999) 85–97.
[16] T. Pretorius, E. Nembach, Acta Mater. 49 (2001) 1971–1980.
[17] E. Orowan, Symposium on International Stresses, Institute of Metal, London, 1947.
[18] J. Moon, S. Kim, J.-I. Jang, J. Lee, C. Lee, Mater. Sci. Eng. A 487 (2008) 552–557.
[19] M. Göken, M. Kempf, Acta Mater. 47 (1999) 1043–1052.
[20] B.-W. Choi, D.-H. Seo, J.-Y. Yoo, J.-I. Jang, J. Mater. Res. 24 (2009) 816–822.
[21] B.-G. Yoo, Y.-J. Kim, J.-H. Oh, U. Ramamurty, J.-I. Jang, Scripta Mater. 61 (2009) 951–954.
[22] R.L. Narayan, K. Boopathy, I. Sen, D.C. Hofmann, U. Ramamurty, Scripta Mater. 63 (2010) 768–771.
[23] K.L. Johnson, J. Mech. Phys. Solids 18 (1970) 115–126.